Torsional Shear and Triaxial Compression Tests on Deformation Characters of Sands Before and After Liquefaction

Susumu YASUDA [1], Tamio MASUDA [2], Nozomu YOSHIDA [3]
Hideo NAGASE [4], Hiroyoshi KIKU [5]
Shigeru ITAFUJI [6], Keiichiro MINE [6] and Kazuya SATO [7]

ABSTRACT

The stress–strain relationships of sand after liquefaction were studied by conducting torsional shear and triaxial compression tests under several conditions. A prescribed number of cyclic loadings were applied first, then a monotonic loading was applied in undrained condition. The stress–strain relationships during the monotonic loading are discussed. The stress–strain curves were affected by the accumulated excess pore pressure ratio and by the severity of liquefaction. The shear and secant modulus decreased to less than 1/1000 due to liquefaction. The shear strain increased more than 10% with very low stress in the liquefied specimen. And, there exists a so called "reference strain at resistance transformation, γ_t" which increases with decreases in soil density, severity of liquefaction and fines content, and with increase with confining pressure.

---

[1] Professor, Dept. of Civil Eng., Tokyo Denki University, Saitama, Japan.
[2] Chief of Section, Tokyo Electric Power Co. Ltd., Tokyo, Japan.
[3] Head of Research, Engineering Research Institute, Sato Kogyo Co., Tokyo, Japan.
[4] Associate Professor, Dept. of Civil Eng., Kyushu Institute of Technology, Kitakyushu, Japan.
[5] Research Associate, Dept. of Civil Eng., Yokohama National University, Yokohama, Japan.
[6] Graduate Student, Dept. of Civil Eng., Kyushu Institute of Technology, Kitakyushu, Japan.
[7] Graduate Student, Dept. of Civil Eng., Yokohama National University, Yokohama, Japan.

INTRODUCTION

It is necessary to know the post liquefaction behavior of sand to estimate large displacement of ground or the settlement of structures due to liquefaction. However, this behavior has not been clarified because studies on liquefaction have focussed mainly on methods to estimate the occurrence of liquefaction.

Therefore, the stress–strain relationships of sand after liquefaction were studied by conducting torsional shear and triaxial compression tests under several conditions of density, confining pressure, fines content and severity of liquefaction. In the tests, a prescribed number of cyclic loading was applied to induce a prescribed excess pore water pressure. Then, a monotonic shear stress was applied.

TEST APPARATUS

Figure 1 shows the torsional shear test apparatus used in this study. Torsional test specimens were hollow cylinders of 10 cm in outer diameter, 6 cm in inner diameter and 10 cm in height. Torsional shear stress was applied at the top of specimens in a horizontal direction with rotational movement of a vertical plunger rod. The rotational movement of the rod was generated with a loading cylinder in cyclic shear stress and with an electric motor in monotonic shear tests. Torsional force, rotational angle and pore water pressure were measured by a torque pick up, a potentiometer and a pressure transducer, respectively. One pair of gap sensors were also used for measuring very small rotational angles.

In triaxial compression tests, column cylindrical specimen of 7.5 cm in diameter and 15 cm in height were used. Axial force, axial displacement and pore water pressure were measured by a road cell, a differential displacement transducer and a pressure transducer, respectively.

TEST CONDITIONS

The sands used in this study were Toyoura sand (G_s=2.64, e_{max}=0.977, e_{min}=0.605, D_{50}=0.16mm, and no content finer) and Narita sand (G_s=2.70, e_{max}=1.371, e_{min}=0.773 D_{50}=0.12mm, and a fine content of 15.2%), as shown in Fig.2.

Most tests were performed using Toyoura sand, which is the standard sand in Japan. The tests were conducted under the following test conditions to clarify the effects of density, confining pressure, excess pore pressure, fines content and severity of liquefaction.

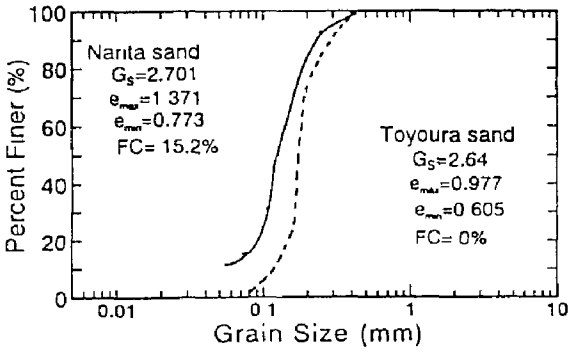

Fig.2 Grain size distribution curves of Toyoura sand and Narita sand

In torsional shear tests

(1) relative density: Dr=0%, 30%, 50% and 70%

(2) effective confining pressure: σ_c' =0.25 kgf/cm^2, 0.5 kgf/cm^2 and 1.0 kgf/cm^2

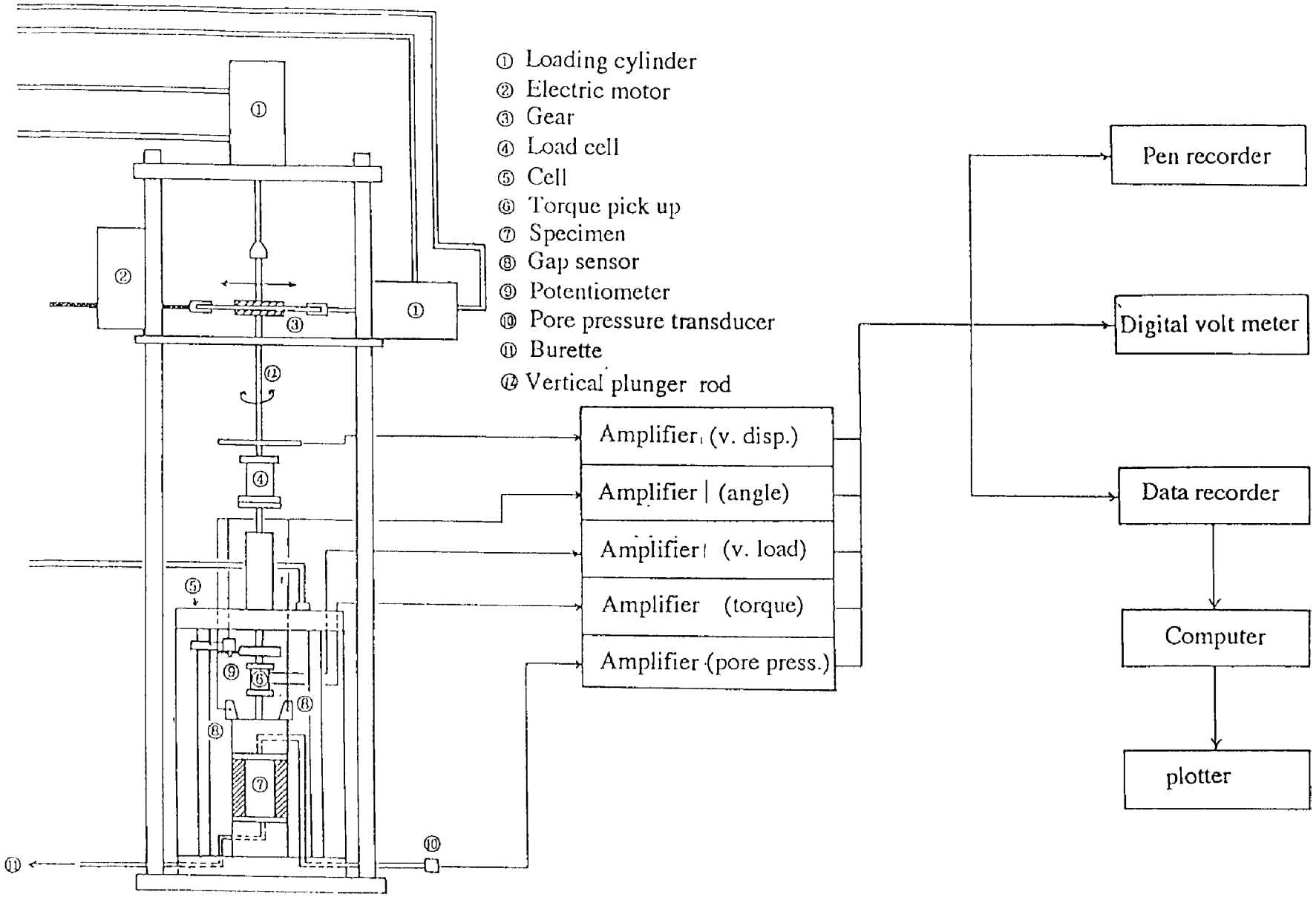

Fig.1 Torsional shear test apparatus

Table 1 Test conditions

No.	Test Device	Sand	Dr %	σ_0' kgf/cm²	$\Delta u/\sigma_v'$ or F_L	No.	Test Device	Sand	Dr (%)	σ_0' kgf/cm²	$\Delta u/\sigma_v'$ or F_L
1	Torsional	C	-1.9	0.5	0	37	Torsional	C	65.4	1.0	0
2	Torsional	C	-5.2	0.5	1.0(F_L=1.0)	38	Torsional	C	73.5	1.0	0.9
3	Torsional	C	29.9	0.5	0	39	Torsional	C	71.9	1.0	1.0(F_L=1.0)
4	Torsional	C	32.6	0.5	1.0(F_L=1.0)	40	Torsional	C	69.4	1.0	1.0(F_L=0.95)
5	Torsional	C	30.5	0.5	1.0(F_L=0.95)	41	Torsional	C	69.9	1.0	1.0(F_L=0.9)
6	Torsional	C	29.2	0.5	1.0(F_L=0.9)	42	Torsional	C	34.7	0.25	0
7	Torsional	C	31.5	0.5	0.3	43	Torsional	C	31.9	0.25	0.9
8	Torsional	C	30.3	0.5	0.6	44	Torsional	C	31.9	0.25	1.0(F_L=1.0)
9	Torsional	C	34.7	0.5	0.9	45	Torsional	C	33.4	0.25	1.0(F_L=0.95)
10	Torsional	C	55.2	0.5	0	46	Torsional	C	33.2	0.25	1.0(F_L=0.9)
11	Torsional	C	53.9	0.5	1.0(F_L=1.0)	47	Torsional	C	45.5	0.25	0
12	Torsional	C	51.7	0.5	1.0(F_L=0.95)	48	Torsional	C	53.5	0.25	0.9
13	Torsional	C	53.1	0.5	1.0(F_L=0.9)	49	Torsional	C	50.0	0.25	1.0(F_L=1.0)
14	Torsional	C	48.3	0.5	0.6	50	Torsional	C	53.1	0.25	1.0(F_L=0.95)
15	Torsional	C	53.0	0.5	0.9	51	Torsional	C	47.9	0.25	1.0(F_L=0.9)
16	Torsional	C	68.2	0.5	0						
17	Torsional	C	69.9	0.5	1.0(F_L=1.0)	52	Triaxial	C	27.8	0.5	0
18	Torsional	C	71.3	0.5	1.0(F_L=0.95)	53	Triaxial	C	28.2	0.5	0.36
19	Torsional	C	68.4	0.5	1.0(F_L=0.9)	54	Triaxial	C	25.3	0.5	0.52
20	Torsional	C	70.2	0.5	0.6	55	Triaxial	C	26.1	0.5	0.9
21	Torsional	C	71.8	0.5	0.9	56	Triaxial	C	23.2	0.5	1.0(F_L=1.0)
22	Torsional	C	-2.2	1.0	0	57	Triaxial	C	49.5	0.5	0
23	Torsional	C		1.0	0.9	58	Triaxial	C	46.4	0.5	0.26
24	Torsional	C	-3.6	1.0	1.0(F_L=1.0)	59	Triaxial	C	49.3	0.5	0.38
25	Torsional	C	-4.6	1.0	1.0(F_L=0.95)	60	Triaxial	C	48.7	0.5	0.94
26	Torsional	C	-4.8	1.0	1.0(F_L=0.9)	61	Triaxial	C	48.0	0.5	1.0(F_L=1.0)
27	Torsional	C	32.7	1.0	0	62	Triaxial	F	38.6	0.5	0
28	Torsional	C	34.5	1.0	0.9	63	Triaxial	F	38.0	0.5	0.44
29	Torsional	C	25.3	1.0	1.0(F_L=1.0)	64	Triaxial	F	39.9	0.5	0.56
30	Torsional	C	25.8	1.0	1.0(F_L=0.95)	65	Triaxial	F	38.8	0.5	0.9
31	Torsional	C	27.3	1.0	1.0(F_L=0.9)	66	Triaxial	F	38.0	0.5	1.0(F_L=1.0)
32	Torsional	C	51.4	1.0	0	67	Triaxial	F	54.8	0.5	0
33	Torsional	C	53.3	1.0	0.9	68	Triaxial	F	54.8	0.5	0.40
34	Torsional	C	46.4	1.0	1.0(F_L=1.0)	69	Triaxial	F	53.3	0.5	0.56
35	Torsional	C	51.0	1.0	1.0(F_L=0.95)	70	Triaxial	F	49.6	0.5	0.9
36	Torsional	C	45.9	1.0	1.0(F_L=0.9)	71	Triaxial	F	53.0	0.5	1.0(F_L=1.0)

sand: C: Clean sand (Toyoura sand)
F: Sand with fines (Narita sand)

(3) excess pore pressure ratio: $\Delta u/\sigma_0' = 0$, 0.3, 0.6, 0.9 and 1.0
(4) severity of liquefaction: $F_L = 1.0$, 0.95 and 0.9

Special tests were also carried out in which the excess pore pressure dissipated after liquefaction up to $\Delta u/\sigma_0' = 0.9$ or 0.6 by drainage, then monotonic shear stresses were applied. The test conditions of all the specimens are listed in Table 1.

In triaxial compression tests
(1) relative density: Dr= 30% and 50%
(2) effective confining pressure: $\sigma_0' = 0.5$ kgf/cm^2
(3) excess pore pressure ratio: $\Delta u/\sigma_0' = 0$, 0.4, 0.6, 0.9 and 1.0
(4) fines content: FC=0% (Toyoura sand) and 15.2% (Narita sand)

TEST PROCEDURES

Sample preparation technique

In the tests for relative densities of 30%, 50% and 70%, specimens were prepared by the air–pluviation method; pouring dry sand into molds through a funnel from constant heights. The density of the specimens was controlled by the height. In the tests for 0% relative density, which is very loose, a special technique for preparing the specimen. was adopted; a slightly wet sand with 1–2% moisture content was carefully filled into a mold without tamping. After being saturated, samples were consolidated isotropically at a prescribed effective confining pressure($\sigma_0' = 0.25$, 0.5 and 1.0 kgf/cm^2) with a back pressure, σ_{BP}, of 2.0 kgf/cm^2 in undrained condition.

Loading pattern in torsional shear tests

In torsional shear tests, a prescribed number of cyclic loading of 0.1 Hz was applied to the specimens in undrained conditions. The cyclic loading was terminated when the excess pore pressure ratio, or FL, reached a prescribed value. Then, a monotonic loading was applied during undrained condition with a relatively high speed of $\gamma = 10\%$ in a minute, as shown in Fig. 3. The amplitude of cyclic loading was controlled to a prescribed value which produced liquefaction in 20 cycles. Therefore, the amplitude of each density was different.

If the number of cycles of cyclic loading was less than 20, liquefaction did not occur However, the stress–strain relationships during the monotonic loading were affected by the excess pore pressure induced during the cyclic loading. Cyclic loading was terminated when $\Delta u/\sigma_0'$ reached 0 or 0.3, 0.6, 0.9, 1.0. The number of cycles was 0 when $\Delta u/\sigma_0' = 0$ and 20 when $\Delta u/\sigma_0'$ was 1.0.

On the contrary, liquefaction occurred when the number of cycles during the cyclic loading exceeded 20, and the severity of liquefaction increased with the number of cycles. The severity of liquefaction was indicated by the factor of safety against liquefaction, FL, in this study. If the number of cycles, N, was 20, FL equalled 1.0. In the case of

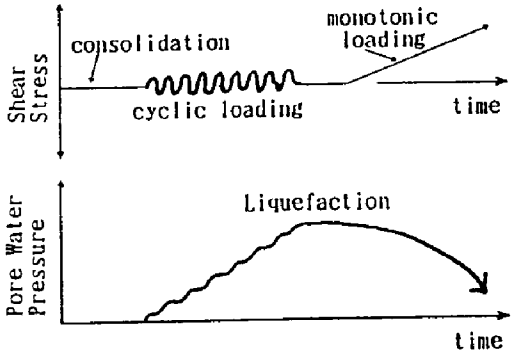

Fig.3 Procedure of cyclic loading and monotonic loading

N>20, N for prescribed FL can be calculated by the following equation, which was derived based on the normalizing method proposed by Tatsuoka et al.(1980).

$$N=20\,(FL)^{1/b} \qquad (1)$$

where: b=−0.17 in clean sand

Therefore, cyclic loading was terminated at N=27 and N=37 in FL=0.95 and FL=0.9, respectively.

Figure 4 shows shear resistance of inner and outer menbrane without a specimen. The shear resistance of membranes was deducted from the measured shear stress.

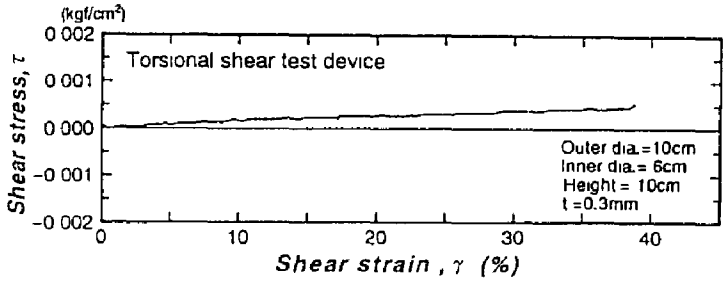

Fig.4 Shear resistance of inner and outer membranes

Loading pattern in triaxial compression tests

In triaxial compression tests, the number of cycles of cyclic loading was fixed for 20 cycles in all specimens. The amplitude of the cyclic loading was controlled to accumulate a prescribed value of excess pore pressure. Therefore, in case of fully−liquefied condition, FL=1 and $\Delta u/\sigma_0' = 1.0$, the cyclic shear stress ratio which produce liquefaction in 20 cycles, $R_{l,20}$, was applied. If the amplitude of cyclic loading was smaller than $R_{l,20}$, liquefaction did not occur and the accumulated excess pore pressure ratio was less than 1.0.

TEST RESULTS

Test Results for Different Pore Pressure Ratio

Relationships among shear stress, τ ,excess pore pressure, Δu, and shear strain, γ , in the monotonic loading are discussed in this study. Figure 5 shows the stress−strain curves and the excess pore pressure−strain curves in the case of $\Delta u/\sigma_0'=0$. Shear stress increased rapidly with shear strain up to $\gamma \fallingdotseq 1\%$. Then, the shear stress increased gradually with shear strain in the cases of Dr ≧ 30%.

On the contrary, the shear stress decreased gradually in the case of Dr=−1.9%. Pore pressure increased with shear strain up to $\gamma \fallingdotseq 2\%$, then decreased, in the cases of Dr ≧ 30%. However, the pore water pressure did not decrease in the case of Dr=−1.9%.

Figure 6 compares the

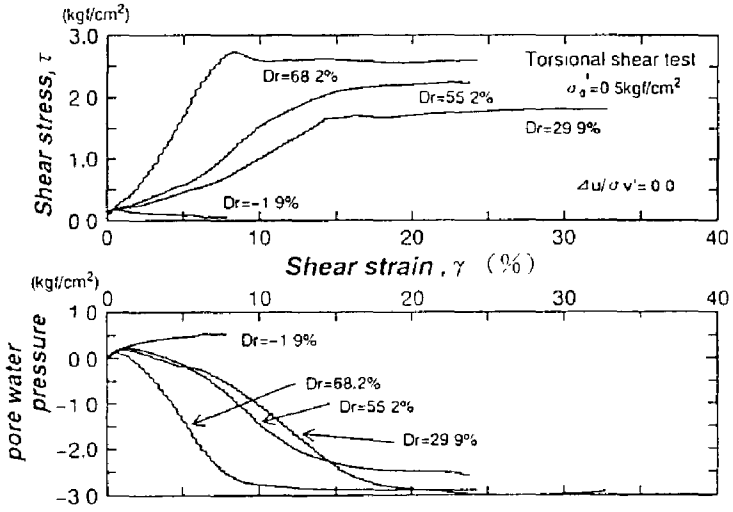

Fig.5 Stress−strain curves and strain−pore pressure curves ($\Delta u/\sigma_0'$=0,static)

stress paths of tests shown in fig. 5. It can be seen that the stress path of Dr=−1.9% proceeded toward the origin of the coordinate axes after having a peak value of shear stress.

Figure 7(a) and Figure 7(b) in which the scales of the axes are enlarged, show stress−strain curves and excess pore water pressure−strain curves in the case of $\Delta u/\sigma_0'$ =1.0 and FL=1.0. Shear strain increased with very low shear stress up to γ >10%. Then, after a resistance transformation point the shear stress increased comparatively rapidly with shear strain, following the decrease of pore water pressure in the cases of Dr ≧ 30%. However, quite little shear stress was generated up to γ =47% without dropping the pore water pressure in the case of Dr=−5.2%.

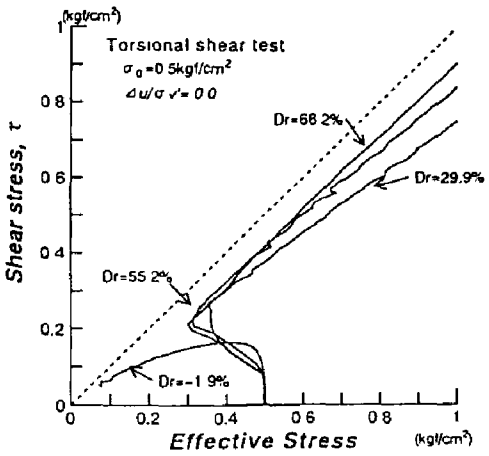

Fig.6 Comparison of stress paths in different densities

Figure 8(a), (b) and (c) compare the stress−strain curves in different pore water pressure ratios and FLs. As shown in these figures, shear stress in some shear strain decreased with the pore water pressure ratio.

Test Results for Different FL

Test results for FL=0.95 and 0.9 are shown in Fig.9(a) and (b). The curves were similar to those of FL=1.0. However, for the similar FL, the resistance transformation point appeared at large strain.

Effect of Drainage

Figure 10(a) and (b) show results of the special tests in which excess pore water pressure dissipated up to $\Delta u/\sigma_0'$=0.9 or 0.6. As shown in these figures, the decreased excess pore water pressure recovered up to $\Delta u/\sigma_0'$=1.0 in small strain. However, shear strains at the resistance transformation points were smaller than those of the data without dissipation.

Effect of Confining Pressure

Figure 11(a), (b), (c) and (d) show the change of stress−strain curves with the development of liquefaction in different confining pressures and relative densities. Comparing the stress−strain curves in the same conditions of relative density and pore pressure ratio, the shear stress in some shear strain increased with the confining pressure when the FL is greater than 1.0. On the contrary, the shear stress in some strain decreased with the confining pressure when the FL is less than 1.0.

Effect of Fine Content

Figure 12(a) and (b) show the relationships between the deviator stress, $\sigma_1-\sigma_3$, and the axial strain, ε, of Toyoura sand during the monotonic loadings using triaxial compression test device. The change of stress−strain curves with different pore pressure ratio in triaxial test were similar to those in torsional test. Figure 13(a) and (b) compare the stress−strain curves of Narita sand, which contains the fines of 15.2%, during the monotonic loading. As shown in Fig 12 and Fig.13, flow deformation was observed also in triaxial tests when the excess pore pressure ratio almost 1.0. The axial strain with low deviator stress was larger in case of clean sand. However, the deviator stress recovered rapidly with axial strain in case of clean sand as compared with that for fine sand.

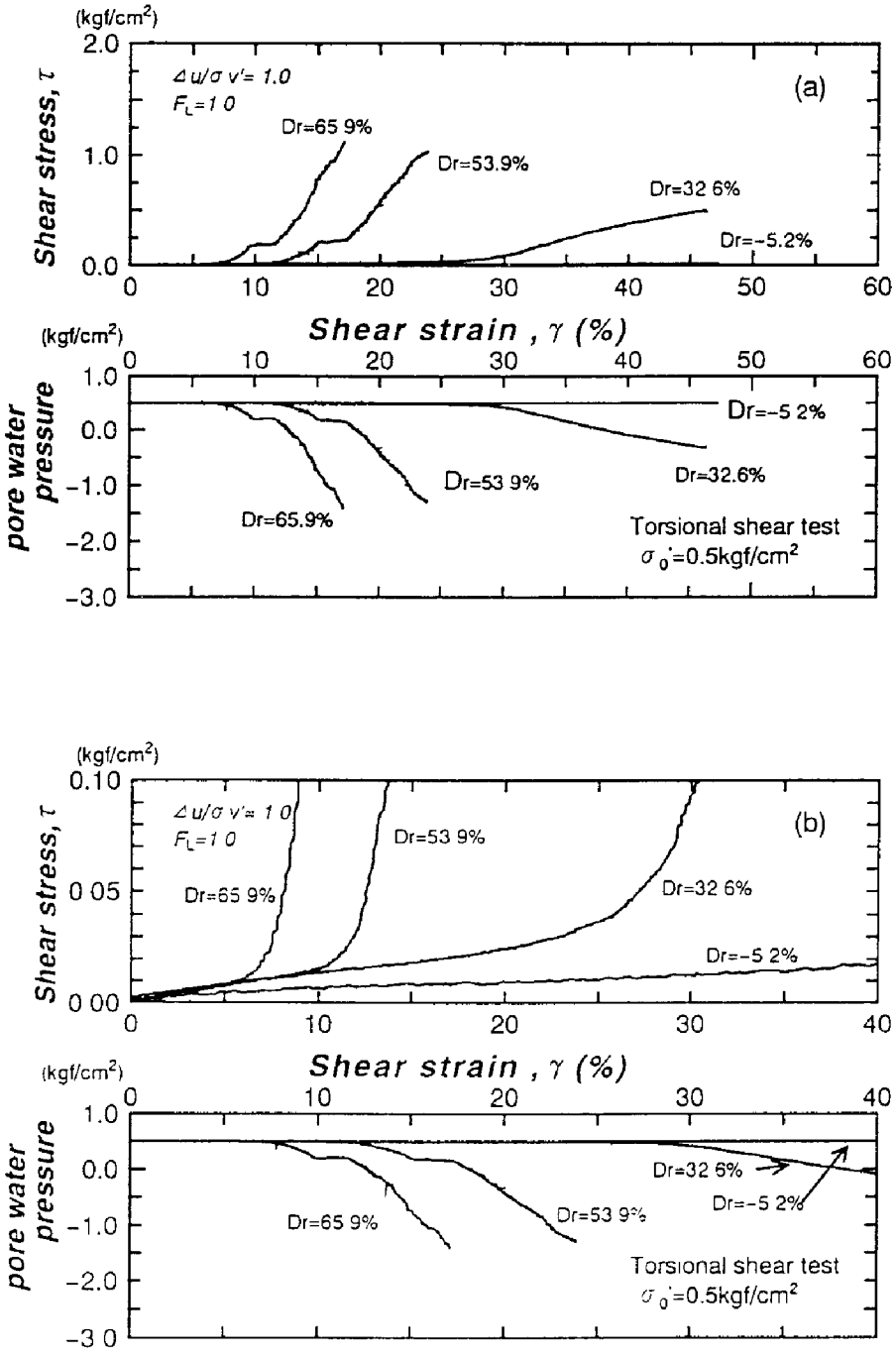

Fig.7 Stress-strain curves and strain-pore pressure curves ($\Delta u/\sigma_0'$=1.0, F_L=1.0)

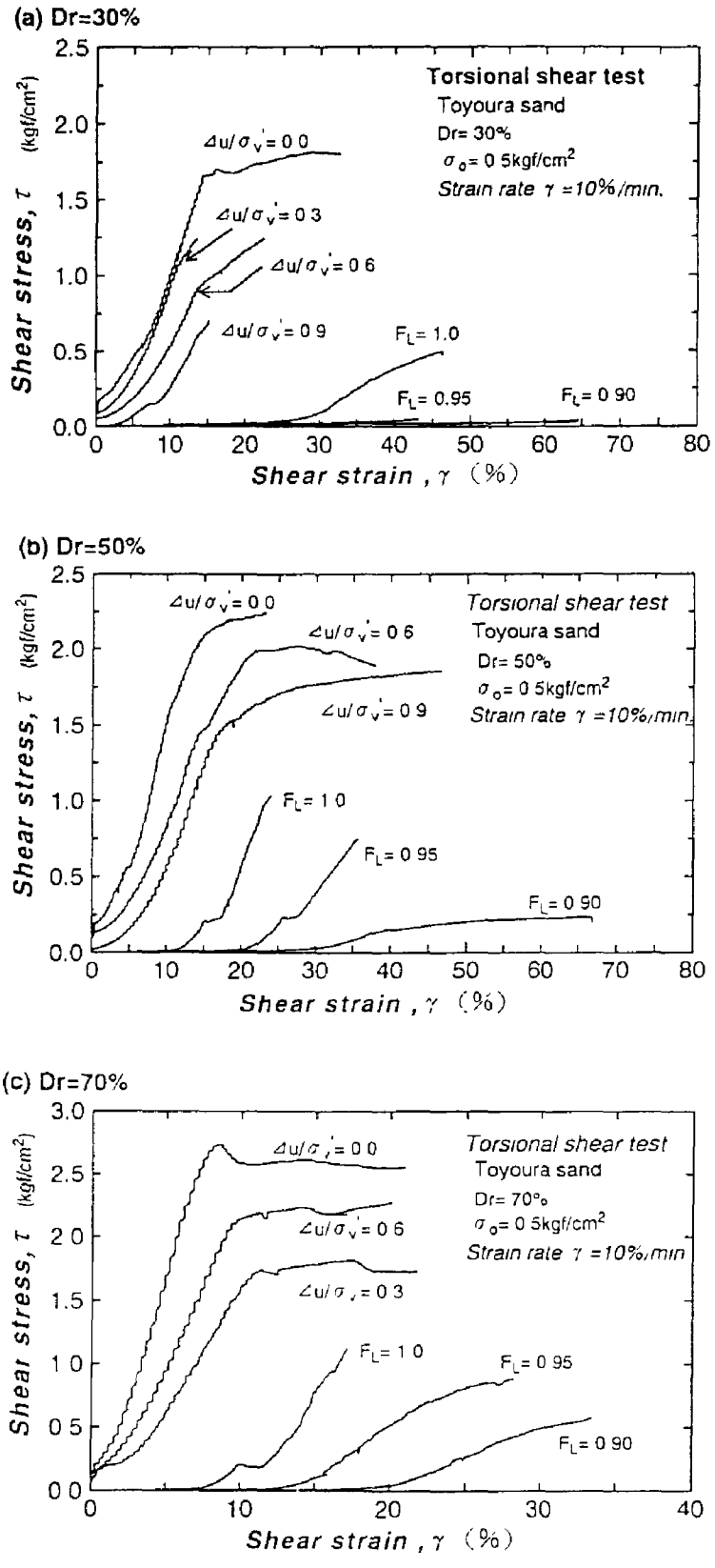

Fig.8 Comparison of stress-strain curves in different densities

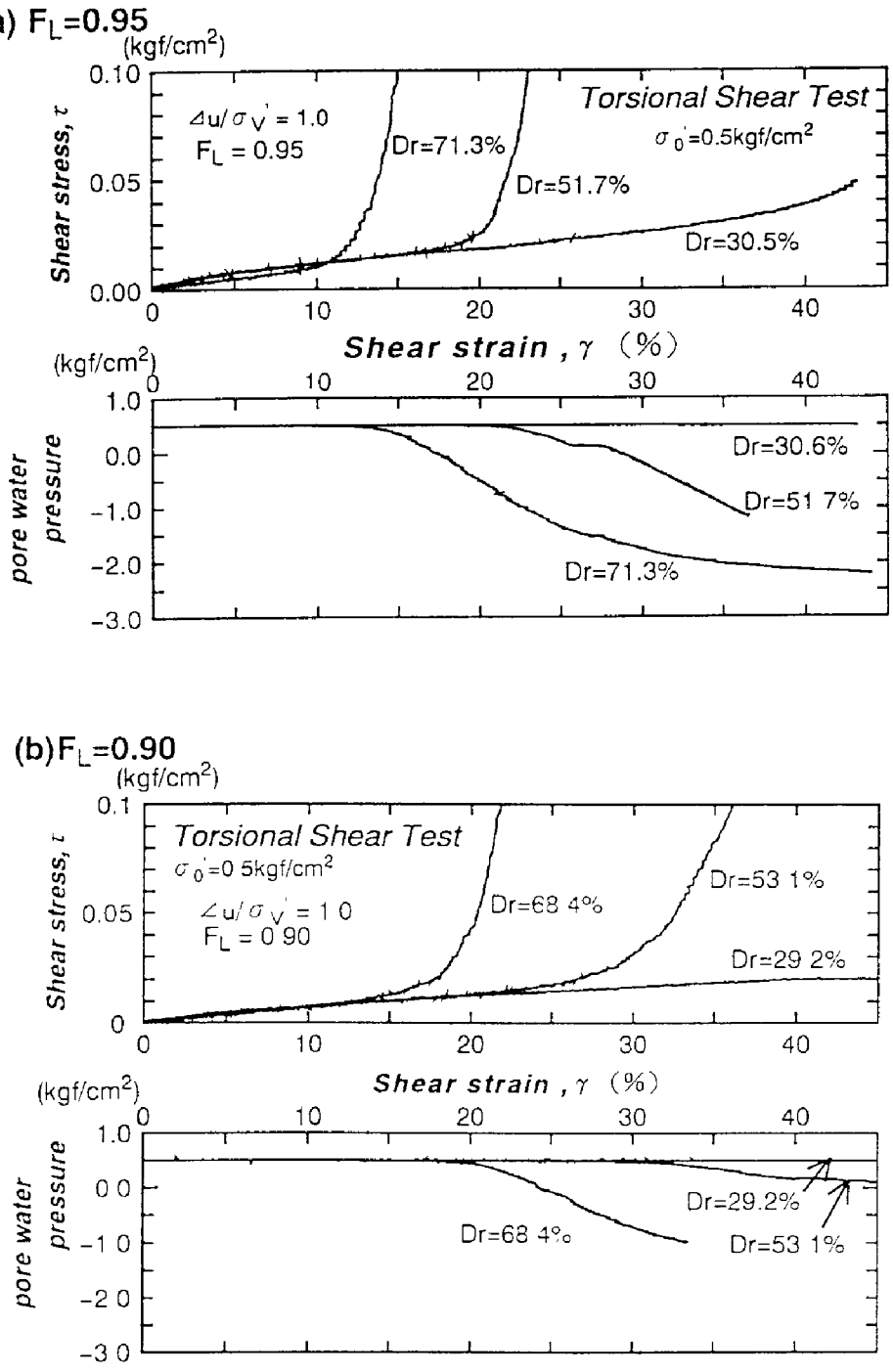

Fig.9 Stress–strain curves and strain–pore pressure curves ($\Delta u/\sigma_0'$=1.0, F_L<1.0)

(a) $\Delta u/\sigma_0' = 1.0 \rightarrow 0.9$

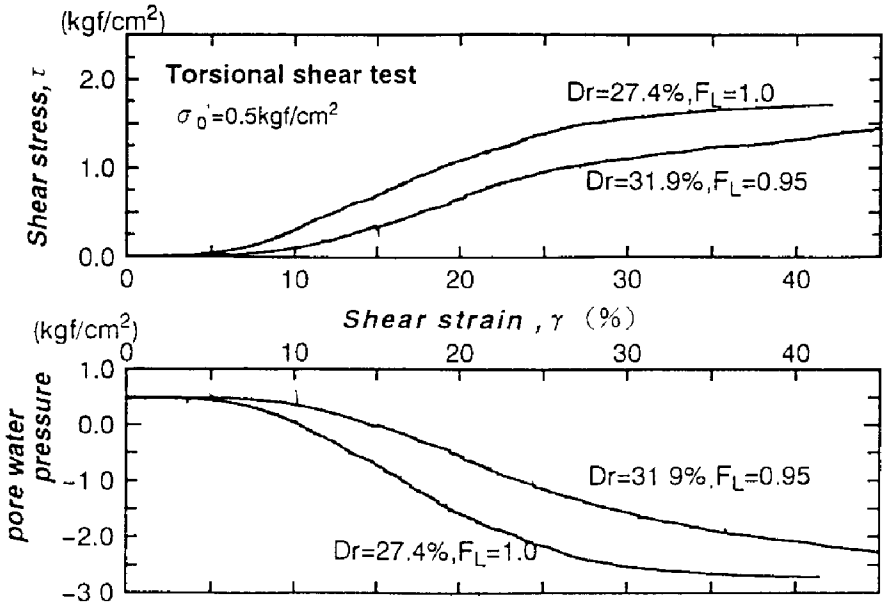

(b) $\Delta u/\sigma_0' = 1.0 \rightarrow 0.6$

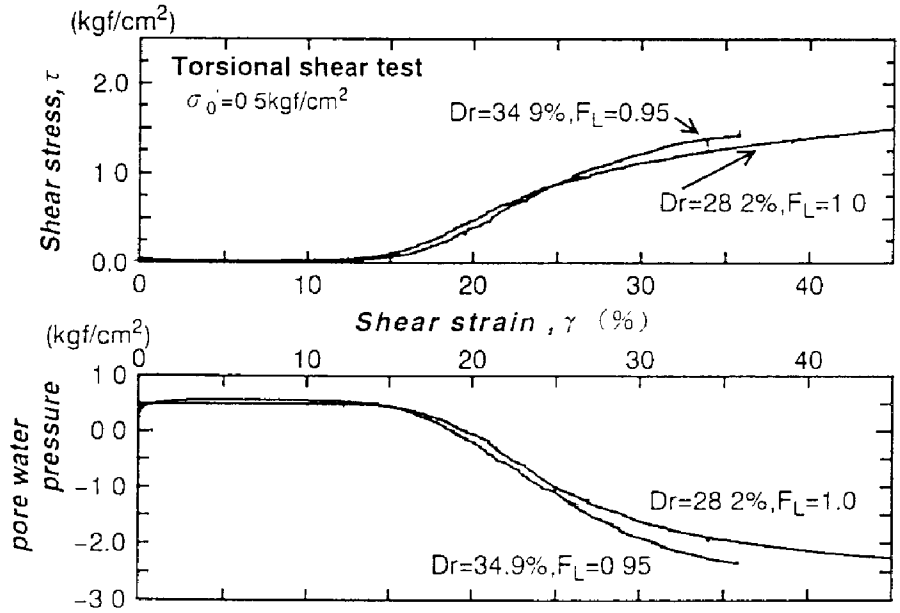

Fig.10 Stress-strain curves and strain-pore pressure curves
($\Delta u/\sigma_0'$=1.0→0.9 or 0.6, F_L=1.0 or 0.9)

(a) Dr=50%, σ_0'=1.0kgf/cm^2

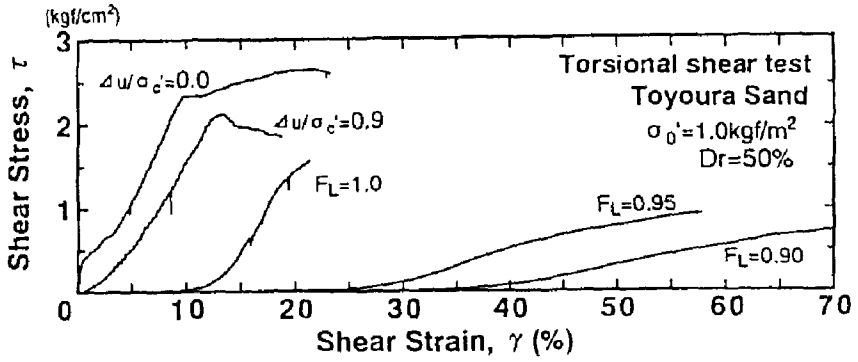

(b) Dr=50%, σ_0'=0.25kgf/cm^2

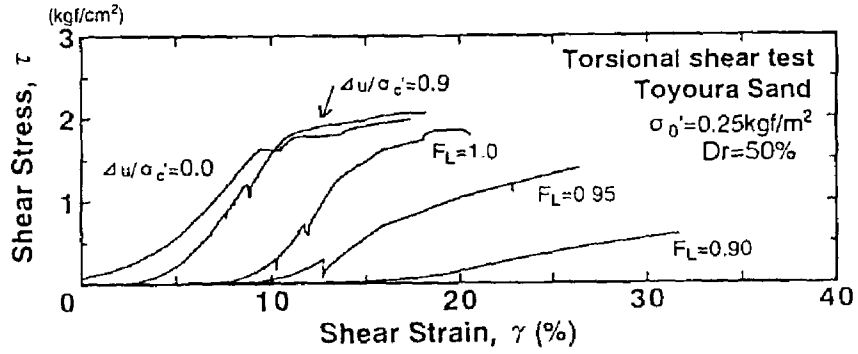

(c) Dr=70%, σ_0'=1.0kgf/cm^2

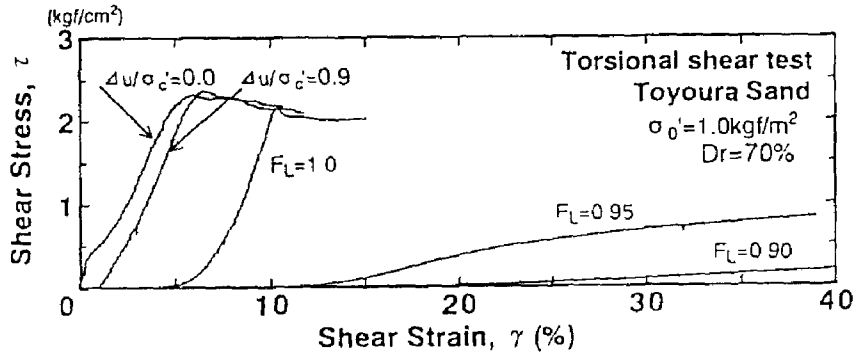

(d) Dr=30%, σ_0'=0.25kgf/cm^2

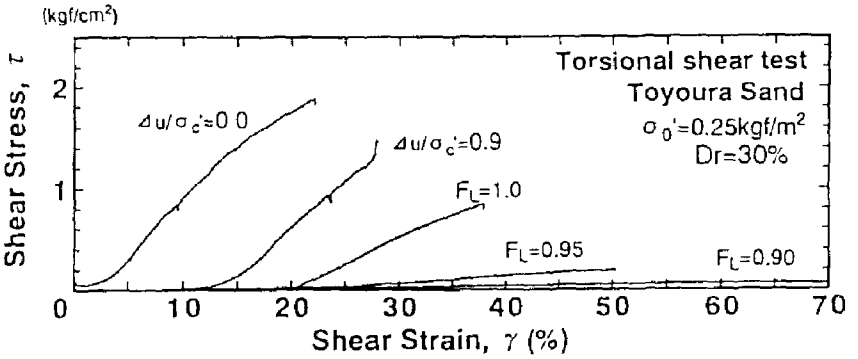

Fig.11 Stress-strain curves in different confining pressures

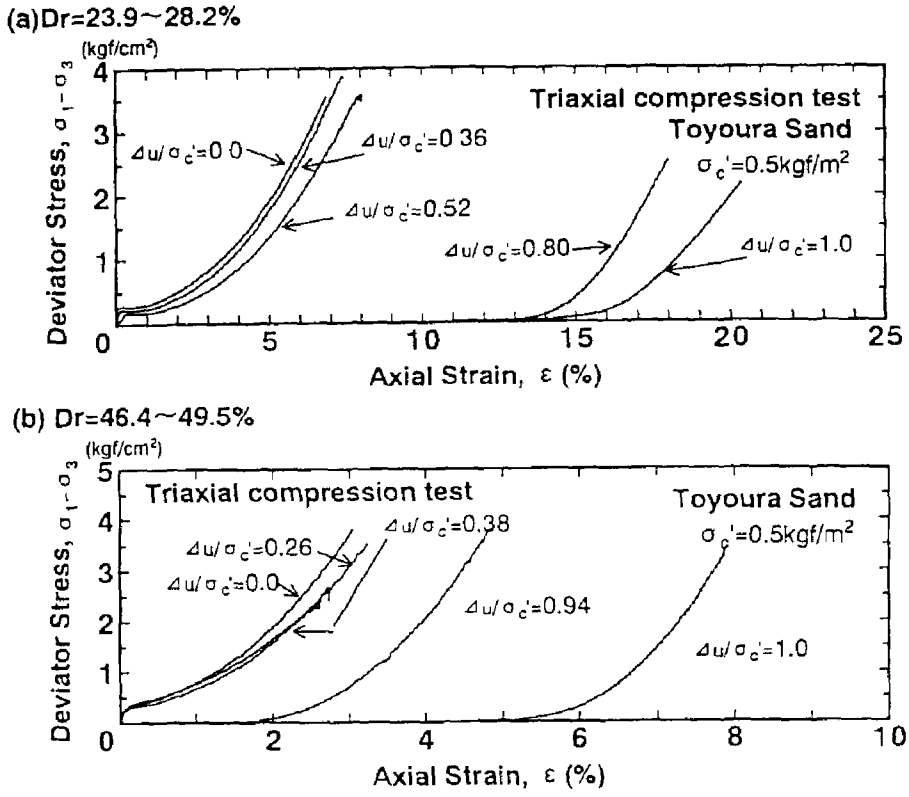

Fig.12 Stress-strain curves in triaxial compression tests (Toyoura sand)

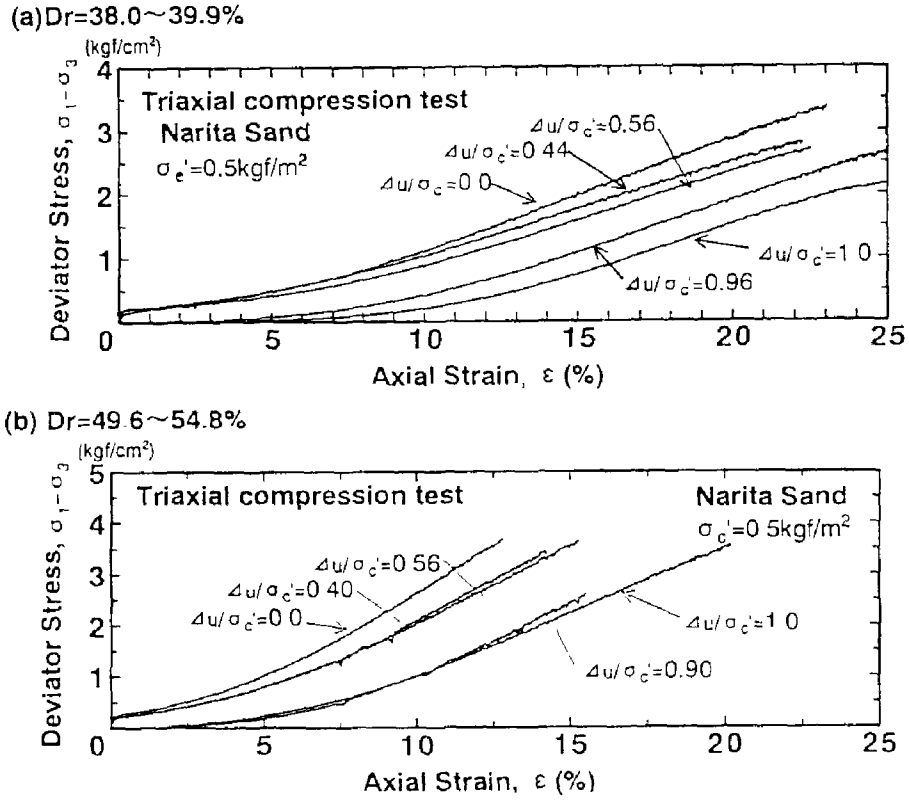

Fig.13 Stress-strain curves in triaxial compression tests (Narita sand)

RELATIONSHIPS BETWEEN $G_1/G_{0.1}$ *AND* $\Delta u/\sigma_0'$ *OR* FL

The rate of reduction of shear modulus, $G_1/G_{0.1}$, was calculated from the torsional test results to know the reduction rate of the rigidity of sand due to liquefaction. $G_{0.1}$ and G_1 were defined as the secant moduli of the stress–strain curves at γ =0.1% in the case of $\Delta u/\sigma_0'$=0 and at γ =0.1 or 1.0, 3.0% in the case of $\Delta u/\sigma_0'$>0, respectively. Figure 14 shows relationships between $G_1/G_{0.1}$ and $\Delta u/\sigma_0'$. It can be seen that $G_1/G_{0.1}$ decreased with an increase in $\Delta u/\sigma_0'$ and reached a vary small value. If the $G_{0.1}$ at γ =0.1% and G_1 at γ =3.0% are assumed as shear moduli of the ground before and after liquefaction, respectively, $G_1/G_{0.1}$ in Fig. 14(a), (b) and (c) are almost 0.001. This means that the shear modulus of the ground decreased to almost 1/1000 due to liquefaction.

Figure 15 shows relationships between FL and $G_1/G_{0.1}$. FL values greater than 1.0 were also calculated by Eq. (1). As shown in this figure, G_1 decreased more than 1/1000 in the range of FL<1.0. Therefore, it can be said roughly that the shear modulus decreases to less than 1/1000 due to severe liquefaction, and varies with the severity of liquefaction.

Yasuda et al. (1992) proposed a simplified analytical method to estimate large ground displacement due to liquefaction. As the parameter G_1/G_0 is used in the method, test results in this study will be utilized in such a kind of analysis.

In the same manner, the rate of reduction of secant modulus, $E_1/E_{0.1}$, was calculated from the triaxial test results. Figure 16(a) and (b) show the relationships between $E_1/E_{0.1}$ and $\Delta u/\sigma_0'$ in Toyoura sand. It can be seen that $E_1/E_{0.1}$ decreased with an increase in $\Delta u/\sigma_0'$ and reached a vary small value, similar in the torsional shear tests. Figure 17(a) and (b) show the relationships between $E_1/E_{0.1}$ and $\Delta u/\sigma_0'$ in Narita sand. The tendency of reduction curves of Narita sand were a little different from those of Toyoura sand, but the obvious difference of the reduction rate between Toyoura sand and Narita sand could not be seen from these figures.

RELATIONSHIPS AMONG γ_L, Dr, FL *AND* σ_0'

As shown in Fig. 7, 8 and 9, shear stress increased comparatively rapidly after a resistance transformation point. The amount of strain up to the resistance transformation point is called here the "value of strain during low resistance, γ_L" as shown in Fig. 18. γ_L thus defined are plotted with Dr and FL in Fig. 19(a), (b) and (c). γ_L increased with decreases in Dr and FL and with increase in σ_0'. In the case of Dr=30%, FL=0.9 and σ_0'=0.5 kgf/cm^2, γ_L reached a very large strain, almost 60%.

A detailed method for the estimation of large ground displacements due to liquefaction based on the γ_L or stress–strain curves studied here will be developed hereafter. However, a simple estimation for permanent ground displacement due to liquefaction is tried here, based on Fig. 19 under the following assumptions;

① A model ground with gentle slope is liquefied from ground surface to the depth of −10m. FL, Dr and unit weight γ_1 of the liquefied layer are 0.95, 30% and 1.9 tf/m^3, respectively.

② Shear strain up to γ_L induces due to liquefaction in the liquefied soil.

Figure 20 shows the distribution of the estimated permanent ground displacement. As shown in this figure, the displacement increases from the bottom of the liquefied layer to the ground surface. And the permanent ground displacement at ground surface can be estimated as 3.5m

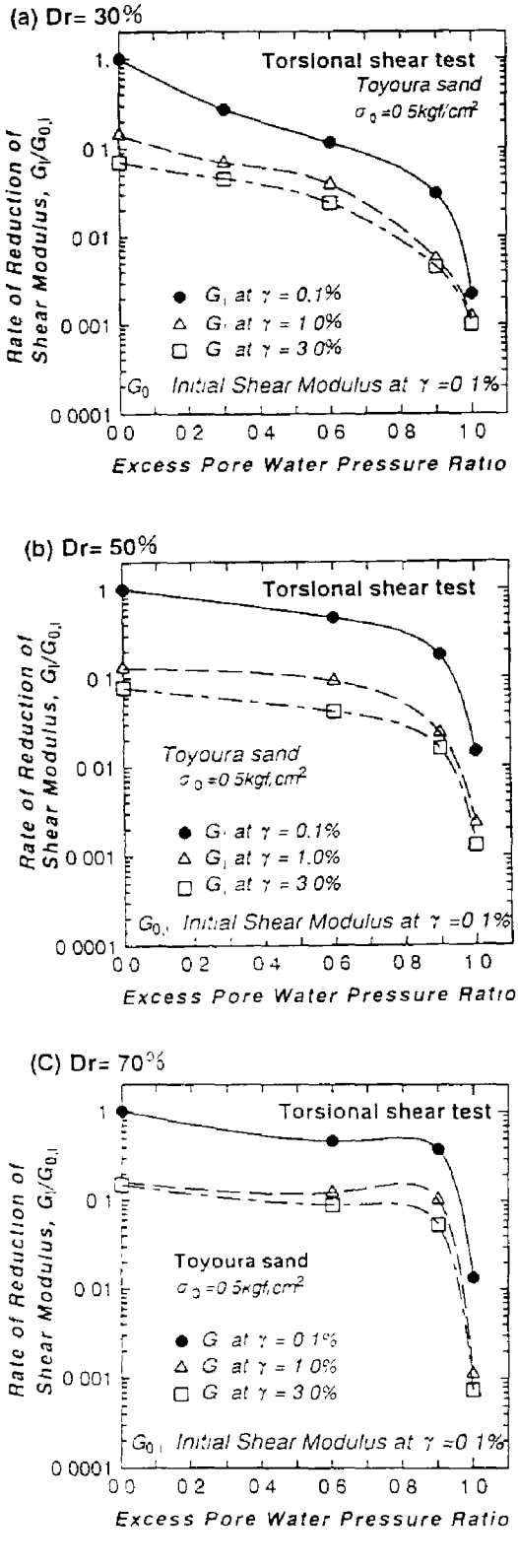

Fig.14 Relationships between $G_l/G_{0,i}$ and $\Delta u/\sigma_0$

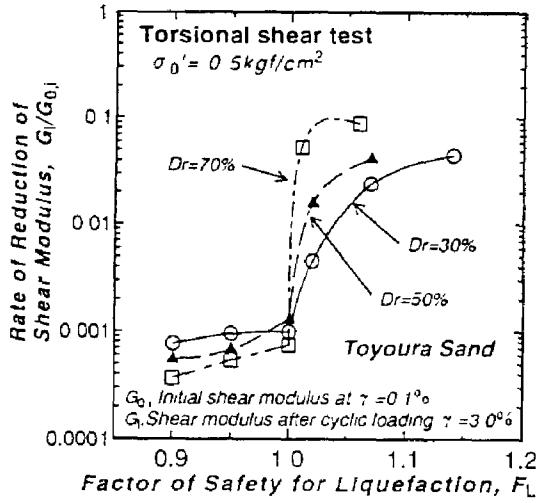

Fig.15 Relationships between $G_l/G_{0,i}$ and F_L

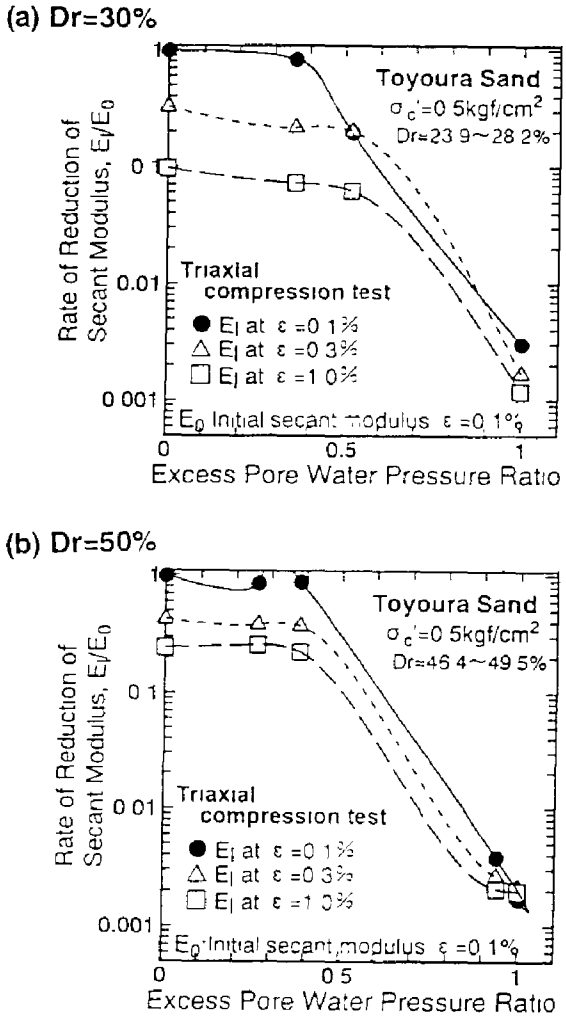

Fig.16 Relationships between $E_l/E_{0,i}$ and $\Delta u/\sigma_0'$

(a) Dr=30%

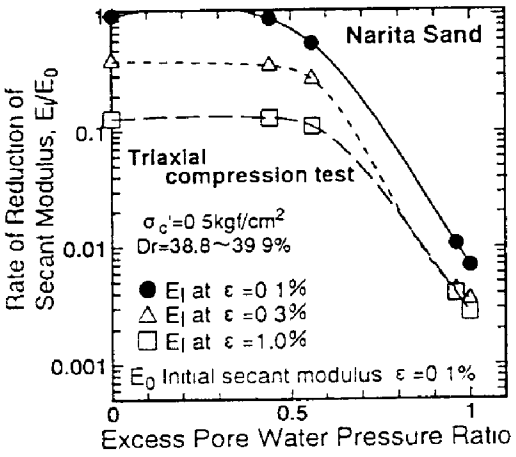

(b) Dr=50%

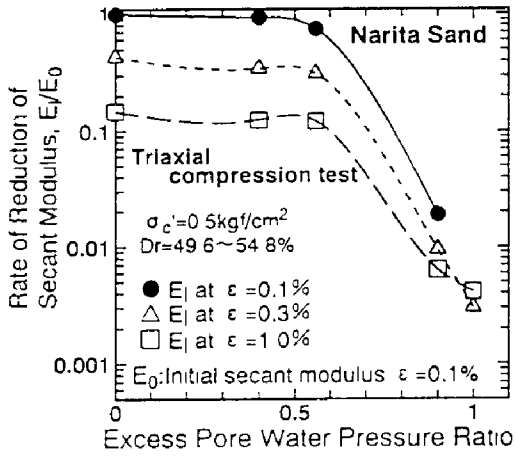

Fig.17 Relationships between $E_l/E_{0,l}$ and $\angle u/\sigma_0'$

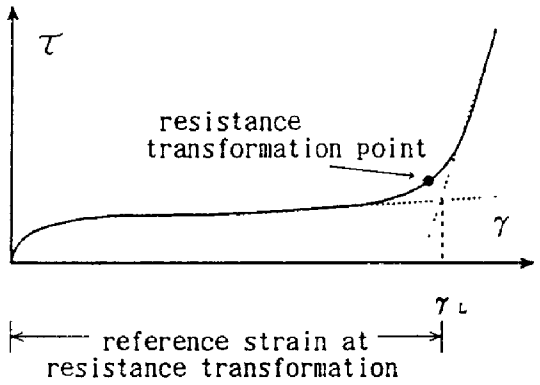

Fig.18 Definition of γ_L

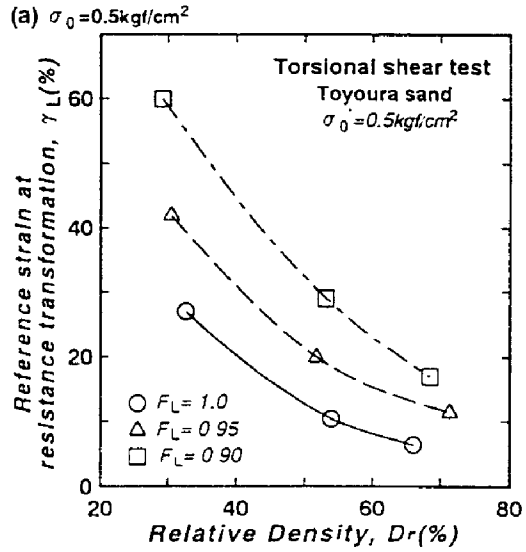

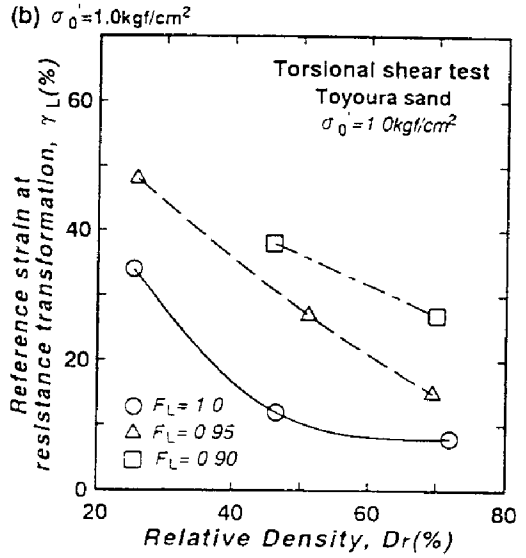

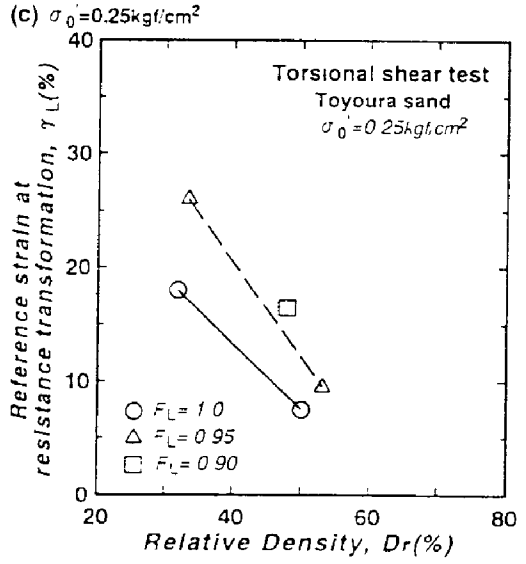

Fig.19 Relationships among γ_L,Dr and F_L

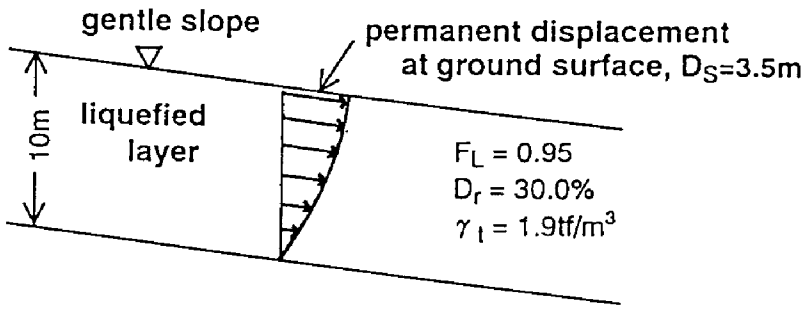

Fig.20 A simple estimation for permanent ground displacement

CONCLUSIONS

Torsional and triaxial shear tests on saturated sands were conducted under several conditions to ascertain the post liquefaction behavior of the sand. The main conclusions are as follows:

(1) stress–strain curves are affected by the excess pore water pressure ratio, $\Delta u/\sigma_0'$, by the factor of safety against liquefaction, FL, and by fine content of the soil.

(2)the shear modulus decreases to 1/1000 or less due to liquefaction and varies with FL.

(3) there exists a so called "reference strain at resistance transformation, γ_t," which increased with decreases in relative density and FL and with increase in with σ_0'.

ACKNOWLEDGEMENTS

Valuable discussions by the members of a committee of the Association for the Development of Earthquake Prediction in Japan. The tests were carried out in the laboratories of Kyushu Institute of Technology and Yokohama National University. The authors would like express their thanks also to Prof. G. Imai of Yokohama National University and Mrs. K. Ushijima of Kyushu Institute of Technology.

REFERENCES

1) Tatsuoka, F., Yasuda, S., Iwasaki, T. and Tokida, K.: Normalized Dynamic Undrained Strength of Sand Subjected to Cyclic and Random Loading, Soils and Foundations, Vol.20, No.3, pp.1–16, 1980.

2) Yasuda, S., Nagase, H., Kiku, H. and Uchida, Y.: The mechanism and A Simplified Procedure for the Analysis of Permanent Ground Displacement due to Liquefaction, Soils and Foundations, Vol.32, No.1, pp.149–160, 1992.